

## ORDER, DISORDER, AND PHASE TRANSITION IN CONDENSED SYSTEM

# Measurement of Density, Temperature, and Electrical Conductivity of a Shock-Compressed Nonideal Nitrogen Plasma in the Megabar Pressure Range

M. A. Mochalov<sup>a</sup>, M. V. Zhernokletov<sup>a</sup>, R. I. Il'kaev<sup>a</sup>, A. L. Mikhailov<sup>a</sup>, V. E. Fortov<sup>b,c</sup>,  
V. K. Gryaznov<sup>c</sup>, I. L. Iosilevskiy<sup>b,d\*</sup>, A. B. Mezhevov<sup>a</sup>, A. E. Kovalev<sup>a</sup>, S. I. Kirshanov<sup>a</sup>,  
Yu. A. Grigor'eva<sup>a</sup>, M. G. Novikov<sup>a</sup>, and A. N. Shuikin<sup>a</sup>

<sup>a</sup> Russian Federal Nuclear Center, Institute of Experimental Physics, Sarov, Nizhni Novgorod oblast, 607188 Russia

<sup>b</sup> Joint Institute for High Temperatures, Russian Academy of Sciences (IVTAN),  
Izhorskaya ul. 13 k. 2, Moscow, 125412 Moscow

<sup>c</sup> Institute of Problems of Chemical Physics, Russian Academy of Sciences, Chernogolovka, Moscow oblast, 142432 Russia

<sup>d</sup> Moscow Institute of Physics and Technology, Institutskii per. 9, Dolgoprudnyi, Moscow oblast, 141700 Russia

\*e-mail: ilios@orc.ru

Received July 24, 2009

**Abstract**—Kinematic and thermodynamic parameters of shock-compressed liquid nitrogen are measured behind the front of a plane shock wave using plane wave and hemispherical shock wave generators. In these experiments, high values of compression parameters (shock-compressed hydrogen density  $\rho \approx 3.25 \text{ g/cm}^3$  and temperature  $T \approx 56000 \text{ K}$  at a pressure of  $P \approx 265 \text{ GPa}$ ) are attained. The density, pressure, temperature, and electrical conductivity of the nonideal plasma of shock-compressed liquid nitrogen are measured. A nearly isochoric behavior of the nitrogen shock adiabat is observed in the pressure range  $P = 100\text{--}300 \text{ GPa}$ . The thermodynamics of shock-compressed nitrogen is analyzed using the model of the equation of state in the quasi-chemical representation (SAHA code) as well as the semiempirical wide-range equation of state developed at the Institute of Experimental Physics. Experimental results are interpreted on the basis of calculations as the fixation of the boundary of transition of shock-compressed nitrogen from the polymer phase to the state of a strongly nonideal plasma at  $P \approx 100 \text{ GPa}$ ,  $\rho \approx 3.4 \text{ g/cm}^3$ .

DOI: 10.1134/S1063776110010097

## 1. INTRODUCTION

The interest in physical properties of compressed and heated hydrogen is primarily due to the presence of nitrogen in nature, in giant planets of the solar system, and in so-called exoplanets (outside the solar system) (see, for example, review [1]), as well as to the abundance of nitrogen in the Earth's atmosphere. It is also due to technical applications of nitrides as ultra-hard refractory materials and, in addition, as one of the main components of disruptive condensed explosives. Molecular nitrogen is characterized by a very high dissociation energy ( $D_2 \approx 9.9 \text{ eV}$ ), which is closer to the ionization energies of the atom and molecules ( $I_a = 14.5 \text{ eV}$ ,  $I_m = 15.6 \text{ eV}$  [2]) as compared to hydrogen. This renders the nitrogen system quite stable to external effects, which follows from the results of static [3–12] and dynamic [13–15] experiments reflecting noticeable structural and electronic transformations in dense nitrogen in the megabar pressure range and in the range of high temperatures ( $kT \sim 1 \text{ eV}$ ). In this paper, we describe the technique and results of measurements of the density, temperature, and conductivity of shock-compressed initially liquid nitrogen in the

range of a nonideal dense plasma in the pressure range  $P \approx 90\text{--}265 \text{ GPa}$  at temperatures  $T \approx (1.5\text{--}60) \times 10^4 \text{ K}$ . In experiments on dynamic compressibility of nitrogen, we used explosive cumulative hemispherical shock wave generators (SWGs) [1, 13, 16]. These generators were employed in experiments on shock compression of dense strongly nonideal nitrogen plasmas [17] in the above pressure and temperature ranges. Analysis of the entire body of experimental data (including our results) and comparison with the results of model calculations make it possible to approximately localize the boundaries of the molecular, polymer, and plasma states of shock-compressed nitrogen.

Kinematic and thermodynamic parameters of shock-compressed liquid nitrogen were measured repeatedly. In [3, 4], these parameters were measured behind the plane shock wave front. Compression of nitrogen up to a density of  $2.8 \text{ g/cm}^3$  was studied in [5–8]. In the pressure range  $P \approx 18\text{--}90 \text{ GPa}$ , temperature  $T \approx (4\text{--}14) \times 10^3 \text{ K}$  and electrical conductivity up to  $5 \times 10^3 (\Omega \text{ m})^{-1}$  were measured. In addition, anomalous “shock-induced cooling” of nitrogen was observed [7, 8]: the nitrogen temperature after the reflection of a shock wave from optical windows



**Table 1.** Experimental values of thermodynamic parameters in the low-temperature range of shock-compressed nitrogen obtained for plane shock waves

	$D$ , km/s	$U$ , km/s	$P$ , GPa	$\rho$ , g/cm <sup>3</sup>	$T$ , K	$E$ , kJ/g
1	$6.87 \pm 0.07$	3.90	$21.6 \pm 0.3$	$1.87 \pm 0.07$	$4200 \pm 100$	-26.2086
2	$7.20 \pm 0.06$	4.17	$24.4 \pm 0.3$	$1.92 \pm 0.05$	$5100 \pm 150$	-25.1191
3	$8.36 \pm 0.09$	5.0	$33.8 \pm 0.5$	$2.01 \pm 0.07$	$6500 \pm 200$	-21.3136
4	$8.94 \pm 0.15$	5.58	$40.4 \pm 0.8$	$2.15 \pm 0.11$	$7200 \pm 250$	-18.2454
5	$9.60 \pm 0.17$	6.31	$48.8 \pm 1.2$	$2.35 \pm 0.11$	9520	-13.9055

Note: Here and in Table 2,  $D$  and  $U$  are the (wave) velocity of the shock wave front and the (mass) velocity of the substance;  $P$ ,  $T$ ,  $\rho$ , and  $E$  are the pressure, temperature, density, and internal energy (measured from the energy of an ideal atomic gas at  $T = 0$  K) in accordance with the Rankine–Hugoniot relations.

the Grüneisen parameter becomes positive again upon an increase in temperature and pressure accompanied by the predicted decomposition of the polymer phase. The parameters of this transition and the shape of the upper boundary of the region of negative values of the Grüneisen parameter are still unclear.

The polymer state of nitrogen predicted in [21] is assumed to be close to the molecular state judging from the binding energy, but with a richer set of attainable states and hence, under certain conditions, more advantageous in entropy as compared to the traditional liquid state or the crystalline state formed by binary molecules [10–12, 19, 24]. In view of this factor, the ionization of dense nitrogen under pressure is more complicated and diverse as compared to hydrogen [25]. In particular, it can be expected that this process occurs from the polymer and not the molecular phase as in molecular hydrogen. The experimental clarification of this question is one of the main goals of this study.

## 2. EXPERIMENTAL

In shock wave experiments with liquid nitrogen, we used two types of cryogenic targets in planar and hemispherical geometry. Experiments with plane shock waves and with pressures up to 50 GPa were performed on the experimental setup described in our earlier publication [9]. Generators of plane shock waves [10] used in our experiments ensure the acceleration of a steel or aluminum striker up to velocities of 2–6 km/s. The results of these experiments are given in Table 1.

Hemispherical cryogenic targets were obtained by replacing a planar striker and screen in the cryostat [3] by hemispherical counterparts. A fragment of the hemispherical cryogenic target is shown in Fig. 2.

In assembling of cryostats of various sizes and screen materials and with various blocks of powerful explosives, experimental setups of the hemispherical type were constructed with the characteristics matching the MZ-4, MZ-8, and MZ-13 shockwave generators (SWGs) [11]. Such devices were used earlier in

experiments with liquid argon [13] and in our experiments for producing pressures in liquid nitrogen exceeding 90 GPa.

For measuring the average velocity of the shock wave, six pairs of electrical contacts 3 pasted in screen 6 on a fixed base and twelve pairs of contacts 2 located on the inner surface of the screen were used. The shock wave velocity in liquid nitrogen was measured by six pairs of contacts 4 and six symmetrically arranged optical sensors 8 prepared from a quartz fiber 400  $\mu\text{m}$  in diameter, which were fixed at a known distance from the screen. The maximum angle of deviation of the electrical contacts and fibers from the vertical axis was  $36^\circ$ . In addition, six contact sensors 5 were arranged symmetrically along the normal to the surface for measuring velocity  $W$  of the free surface of the steel striker. All contacts were prepared of copper wire 0.15 mm in diameter in enamel insulation. When a shock wave (or the striker) acted on a contact, its insulation was damaged, which resulted in the closure of

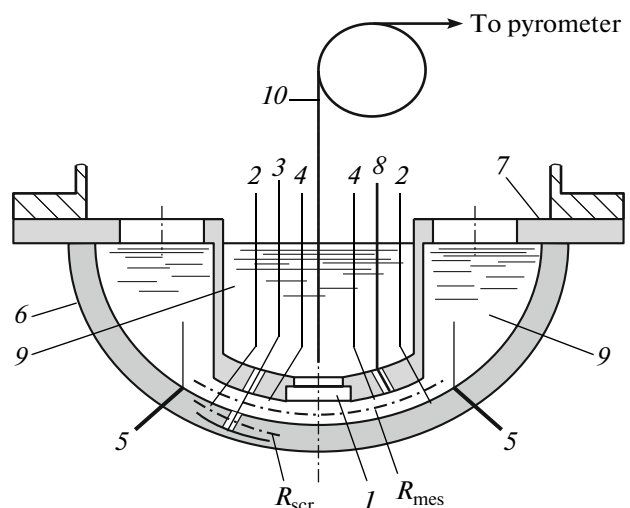


**Fig. 2.** Measuring unit: (1) optical window; (2–5) contacts; (6) screen; (7) holder; (8) optical sensors; (9) liquefied gas; (10) optical fiber.

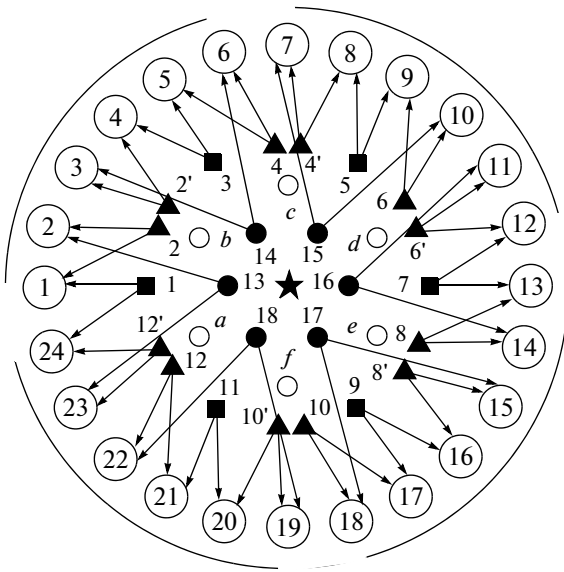


**Fig. 3.** Schematic of contacts sensors (■) in the screen, (▲) on the screen surface, and (●) in the nitrogen) and optical (○) fibers with photodiode, transducers; (★) optical fiber for recording spectral temperatures) sensors in the hemispherical cryogenic unit. Numbers in circles indicate measuring channels.

the circuit in the electrical block forming the pulse corresponding to the arrival of the shock wave at a preset base and detected by the oscilloscope.

Optical sensors 8 and photodiode transducers registered the glow of the shock wave front at the exit of the shock wave from the screen until the beam was cut off at the surface of the sapphire window (or at the endface of sensor 8). For the known base of arrangement of sensors 8, this allowed us to measure additionally the velocity of the shock wave in liquid nitrogen.

Radiation emitted by the shock wave front through optical window 1 via fiber 10 located in the bulk of liquid nitrogen along the cryogenic cell axis was detected simultaneously in five spectral ranges by a visible-range pyrometer combined with high-speed oscilloscopes. The spectral temperatures of the shock wave front and the time of propagation of the shock wave in liquid nitrogen were measured from the recorded oscillograms. Figure 3 shows the arrangement of contacts and optical sensors.

Liquid nitrogen was poured into the cryostat immediately before the experiment. Air around the cell with liquid nitrogen was evacuated to a residual pressure of less than 10 Torr. Initial temperature  $T_0 = 77$  K of liquid nitrogen was monitored by a calibrated platinum thermometer. Measured temperature  $T_0$  corresponds to liquid nitrogen density  $\rho_0 = 0.807$  g/cm<sup>3</sup>.

### 3. MEASUREMENT OF DYNAMIC CHARACTERISTICS OF SHOCK COMPRESSION

Figure 4a shows a typical oscillogram of closure of contacts behind the shock wave front. The velocity of the shock wave front was determined from the difference of the times of propagation of the shock wave in the screen,  $\Delta t_{\text{scr}} = t_2 - t_1$ , and in liquid nitrogen,  $\Delta t_{\text{N}_2} = t_3 - t_2$ , on the known bases, which was measured in each measuring channel separately. The results were averaged. Figure 4b shows the luminescence oscillogram of the shock wave front, recorded with the help of an optical sensor and a photodiode detector. The time of propagation of the shock wave in liquid nitrogen in this case was determined from the difference  $\Delta t_{\text{N}_2} = t_4 - t_0$ .

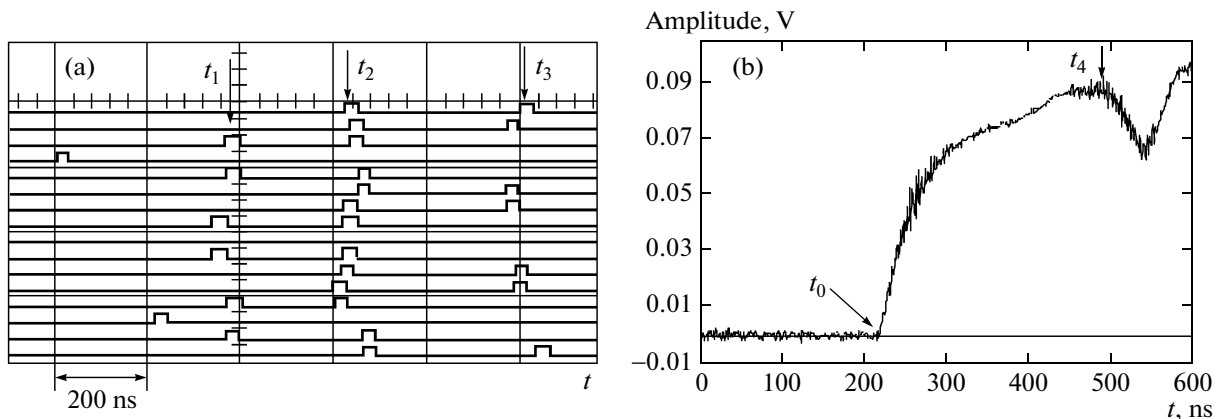


**Fig. 4.** Fragments of oscillograms of signals recorded by (a) electric contact and (b) optical sensors in experiment with the MZ-4 SWG: pulses from the contacts in the screen ( $t_1$ ), on the screen ( $t_2$ ), and after the passage through the nitrogen layer ( $t_3$ );  $t_0$  is the beginning of luminescence of the shock wave front in nitrogen;  $t_4$  is radiation cutoff at the endface of optical sensor 8 (see Fig. 2).

In accordance with reflection method, pressures and mass velocities in the direct wave can be determined from the measured velocity of the shock wave in nitrogen by solving the problem on the decay of an arbitrary discontinuity formed upon the arrival of the shock wave at the aluminum–nitrogen interface. In experiments with generators of plane shock waves, such a problem can be solved easily: it is necessary to measure the velocity of shock waves in the substance under investigation and in the screen and to know the equation of state of the screen. A peculiar feature of experiments with spherical generators is an increase in the shock wave velocity in the sample and in the elements of the setup when the shock wave propagates to the center. The experimentally measured values of average velocities of shock waves have meaning only for radii at the middles of measuring bases of the relevant structural elements.

In this study, the parameters of shock-compressed liquid nitrogen were determined from the conservation laws at the discontinuity decay boundary, formally transferred to radius  $R_{\text{mes}}^{\text{N}_2}$  of the shock wave velocity measurement in nitrogen. For this purpose, we measured the velocity of the shock wave front in nitrogen as well as the velocity of the shock wave front in the screen of the experimental setup, but over radius  $R_{\text{mes}}^{\text{scr}}$  (see Fig. 2); the value of this radius was later corrected theoretically to its value over radius  $R_{\text{mes}}^{\text{N}_2}$ . Technologically, this version of shock wave velocity measurement in the screen is simpler since it does not require the installation of standard specimens in the setup and appears justified since the results for liquid nitrogen were obtained in the range of parameters that has not been investigated before, and the equation of state for the screen (AD1 aluminum) in this pressure range is well known.

To derive analytic dependences  $D(R)$  of the shock wave front velocity in structural elements on the radius and to determine the parameters of state of the screen over the measuring radius  $R_{\text{mes}}^{\text{N}_2}$ , computer simulation of experiments was performed using the 1D gasdynamic program developed at the Institute of Experimental Physics [26]. The parameters of the shock adiabat for aluminum were borrowed from [27] for the initial aluminum density  $\rho_0 = 2.742 \text{ g/cm}^3$  corresponding to the aluminum density at the liquid nitrogen temperature  $T_0 = 77.4 \text{ K}$ . We used in our calculations the equation of state from [28] for the explosive consisting of the trotyl–hexogen alloy (TG25/75) and the equation of state from [29] refined in the high-density region for iron.

Figure 5 shows the results of computer simulation based on the 1D gasdynamic program [14] and experimental parameters of propagation of a shock wave in the screens for MZ-8 and MZ-13 SWGs. It can be seen that the shock wave velocities in the screens mea-

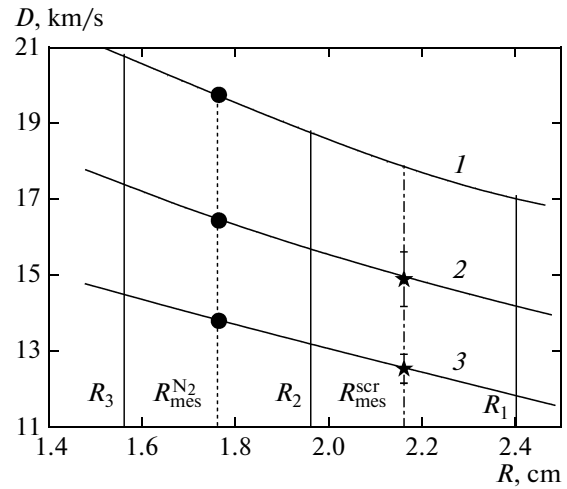


**Fig. 5.** Dependence of the shock wave front velocity on radius in different screens: (1) Al (MZ-13 SWG); (2) Al (MZ-8 SWG); (3) Fe (MZ-8 SWG);  $R_1$  and  $R_2$  are the inner and outer radii of the screen, respectively;  $R_{\text{mes}}^{\text{N}_2}$  and  $R_{\text{mes}}^{\text{scr}}$  are radii of measurement of shock wave parameters in nitrogen and in the screen;  $R_2$ – $R_3$  is the base for measuring the shock wave velocity in liquid nitrogen; (★) experiment; (●) recalculation to  $R_{\text{mes}}^{\text{N}_2}$ , experimental data; curves correspond to calculations.

sured by contacts in experiments with the MZ-8 generator over radius  $R_{\text{mes}}^{\text{N}_2} = 2.16 \text{ cm}$  are in good agreement with the result of gasdynamic calculations. For processing experimental results, we used the values of parameters of the shock wave in screens measured over radius  $R_{\text{mes}}^{\text{N}_2}$ . In accordance with the reflection method, the pressures and mass velocities (velocity of motion of the substance) in nitrogen were determined by solving the system of equations describing isentropes of screen expansion calculated from the states over measuring radius  $R_{\text{mes}}^{\text{N}_2}$  and “wave” beams  $P = \rho_0^{\text{N}_2} U D_{\text{N}_2}$ . The density of shock-compressed liquid nitrogen was determined from the mass conservation law. The results of experiments with liquid nitrogen are given in Table 2, which also contains the measured velocities of shock waves in screens over radius  $R_{\text{mes}}^{\text{scr}}$  and corrected values for radius  $R_{\text{mes}}^{\text{N}_2}$ .

#### 4. MEASUREMENT OF TEMPERATURE AND OPTICAL CHARACTERISTICS OF SHOCK-COMPRESSED NITROGEN PLASMA

Radiation emitted by the shock wave front through optical window 1 (see Fig. 2) was transferred by fiber 10

**Table 2.** Kinematic and thermodynamic parameters of shock-compressed nitrogen plasma obtained in our experiments with hemispherical shock waves in the plasma domain

Measured velocity of shock wave		Parameters of shock wave in screen over radius $R_{mes}^{N_2}$			Parameters of shock wave in nitrogen plasma over radius $R_{mes}^{N_2}$					
$R_{mes}^{scr}$ , mm	$D$ , km/s	$D$ , km/s	$U$ , km/s	$P$ , GPa	$R_{mes}^{N_2}$ , mm	$D$ , km/s	$U$ , km/s	$P$ , GPa	$\rho$ , g/cm <sup>3</sup>	$E$ , kJ/g
1. MZ-4 SWG, Al screen										
32.75	$12.74 \pm 0.42$	13.55	6.12	227.6	29	$12.03 \pm 0.25$	9.11	$88.4 \pm 2$	$3.33 \pm 0.20$	$7.7 \pm 2.9$
2. MZ-8 SWG, Al screen										
21.65	$14.91 \pm 0.71$	16.49	8.50	384.5	17.6	$16.19 \pm 0.36$	12.24	$160 \pm 3$	$3.31 \pm 0.26$	$41.1 \pm 6.7$
3. MZ-8 SWG, Fe screen										
21.65	$12.57 \pm 0.38$	13.85	6.56	715	17.6	$14.60 \pm 0.26$	11.29	$133 \pm 3$	$3.56 \pm 0.14$	$29.9 \pm 3.0$
4. MZ-13 SWG, Al screen										
—	—	19.70	11.20	605.3	17.6	$20.90 \pm 0.68$	15.71	$265 \pm 5$	$3.25 \pm 0.25$	$89.6 \pm 11.0$
5. MZ-8 SWG (with different explosive), Al screen										
21.65	—	17.31	9.18	436	17.6	$17.28 \pm 0.40$	13.14	$183 \pm 6$	$3.37 \pm 0.35$	$52.5 \pm 10.3$

having a diameter of 400  $\mu\text{m}$  and arranged in the bulk of liquid nitrogen along the cryogenic cell axis and by an optical-fiber line to a pyrometer [30], in which it was detected by photoelectric multipliers (PEMs) in a complex with high-speed oscilloscopes at wavelengths  $\lambda = 600, 550, 498, 450$ , and 406 nm selected by interference light filters with a transmittance amplitude of about 50% and a transmission band width  $\Delta\lambda \approx 10$  nm at the half-amplitude level. The optical line was calibrated preliminarily to the standard radiation source. To attenuate radiation, neutral light filters were used with the transmittance measured on a DR-4000U spectrophotometer. Figure 6 shows typical radiation oscillograms of the shock wave front in liquid nitrogen obtained in experiments with MZ-4, MZ-8, and MZ-13 SWGs.

It can be seen that the form of radiation at the shock wave front changes. At a pressure of approximately 90 GPa (Fig. 6a), the sharp increase in the radiation intensity over about 100 ns on segment 0–1 changes to a slower increase during the next 250 ns on segment 1–2. At pressures of 162 (Fig. 6c) and 265 GPa (Fig. 6d), the increasing segment changes to a segment with a practically constant radiation level. The difference in the form of oscillograms can be explained qualitatively by dissociation of nitrogen. In the first case (segment 0–1), the sharp increase in the radiation intensity (and temperature) is associated with ionization of the initial molecules, while the subsequent increase on segment 1–2 can be attributed to ionization of atoms formed as a result of dissociation of molecules. Our calculations (SAHA code) and those performed in [32] show (see Fig. 14 below) that,

at a pressure of 100 GPa, more than half of the molecules have been dissociated, and rapid ionization of atoms begins at pressures close to 130 GPa. This means that the increase in the number of electrons determining the type of radiation is controlled by ionization of molecules and atoms at  $P < 130$  GPa and by atoms alone at higher pressures. The form of radiation from the shock wave front also changes thereby. In data processing for the experiment with the MZ-4 SWG (see Fig. 6a), the amplitudes of radiation on segment 1–2 were averaged.

Figure 7 gives a description of measured spectral temperatures by the Planck function for some experiments with liquid nitrogen. The problem of determining the temperature and emissive power from the experimentally measured spectral fluxes was solved using the nonlinear least squares technique in the model with two parameters ( $T$  and  $\varepsilon$ ) [31]. This necessitates certain assumptions concerning the emissive power of the shock wave front. We assumed here while estimating temperature in a pressure range of up to 170 GPa that the emissive power in the wavelength range being detected is constant ( $\varepsilon = \text{const}$ ). However, we failed to describe the experimental data for the MZ-13 SWG in this approximation since either the emissive power  $\varepsilon$  exceeded unity, or the iterative process did not converge to the exact solution. For this reason, the emissive power for this experiment was chosen in the form  $\varepsilon = \exp(a_0\lambda)$ .

The values of temperatures measured in shock-compressed liquid nitrogen in experiments with plane waves are given above in Table 1. The values of temperature obtained in experiments with hemispherical

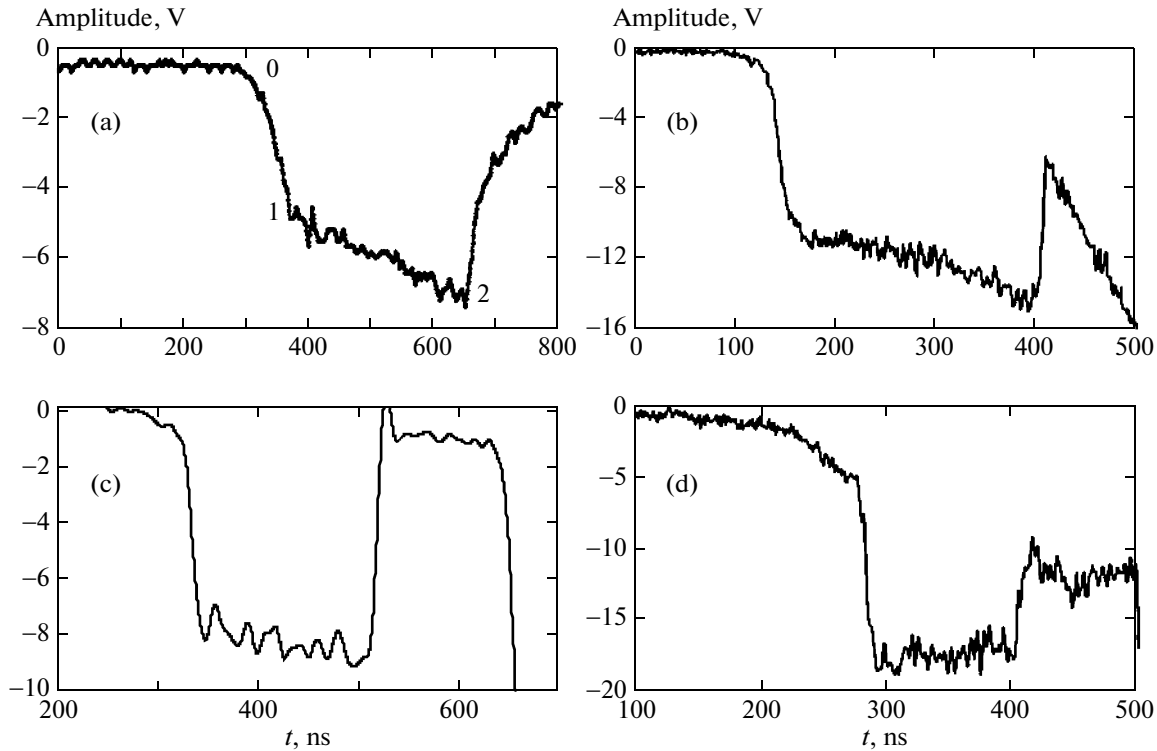


**Fig. 6.** Oscillograms of radiation emitted by the shock wave front in liquid nitrogen: (a)  $\lambda = 498$  nm,  $P = 88.5$  GPa; (b)  $\lambda = 498$  nm,  $P = 133$  GPa; (c)  $\lambda = 406$  nm,  $P = 160$  GPa; (d)  $\lambda = 465$  nm,  $P = 265$  GPa.

shock waves and of the emissive power are given in Table 3 and Fig. 8. For definiteness, the values of temperature are reduced to pressures corresponding to measurements of the shock wave front velocity in nitrogen for  $R_{\text{mes}}^{N_2}$ .

### 5. RESULTS OF MEASUREMENT OF SHOCK-COMPRESSED NITROGEN CONDUCTIVITY

Our experiments were performed on a setup for measuring high electrical conductivity [33] as well as the conductivity of liquefied gases (argon, krypton, and xenon). The experimental dependences of the liquid nitrogen conductivity on the shock wave ampli-

tude are represented in Fig. 9 together with the data obtained in [8].

Owing to high mobility of electrons, the electrical conductivity of liquid nitrogen is predominantly of the electron type. In the density range up to  $2.5$  g/cm<sup>3</sup> studied here, the concentration of nitrogen molecules is  $n = (3-5) \times 10^{22}$  cm<sup>-3</sup>; consequently, the electron mean free path  $l \propto n^{-1/3}$  cm changes insignificantly and remains practically constant ( $l \approx 4 \times 10^{-6}$  cm). For this reason, the observed increase in the conductivity by approximately four orders of magnitude is completely determined by an increase in the electron concentration and weakly depends on the change in the electron mobility; for  $P < 30$  GPa, ionization of mole-

**Table 3.** Temperature of a nonideal plasma of shock-compressed nitrogen

No.	SWG	Screen	$\varepsilon$	$P$ , GPa	$T$ , K
1	MZ-4	Al	$0.32 \pm 0.04$	88.5	$16200 \pm 900$
2	MZ-8	Fe	$0.59 \pm 0.04$	133	$24600 \pm 500$
3	MZ-8	Al	$0.23 \pm 0.12$	160	$28400 \pm 2200$
4	MZ-13	Al	$\exp(-2.07 \times 10^{-3}\lambda)$	265	$56000 \pm 15200$

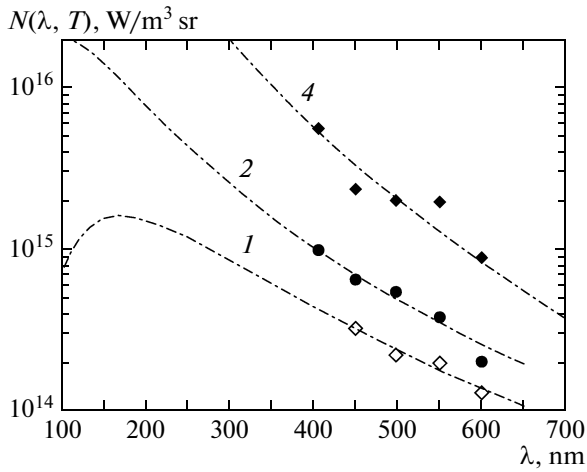


**Fig. 7.** Description of spectral temperatures in shock-compressed liquid nitrogen in various setups (see Table 2) by the Planck function: (1)  $T = 1.7 \times 10^4$  K,  $\varepsilon = 0.28$ ; (2)  $T = 3.03 \times 10^4$  K,  $\varepsilon = 0.204$ ; (4)  $T = 5.6 \times 10^4$  K,  $\varepsilon = \exp(-2.07 \times 10^{-3}\lambda)$ .

cules takes place, while for  $P > 30$  GPa, both molecules and atoms appearing as a result of dissociation of molecular nitrogen are ionized.

The absolute values of conductivity measured here at low pressures of about 20 GPa coincide with experimental data, while those measured at higher pressures slightly exceed the experimental values [8]. This discrepancy can be due to the features of measuring circuits (standard measuring circuit using the standard shunt from [8] and the circuit for measuring high conductivities [33]).

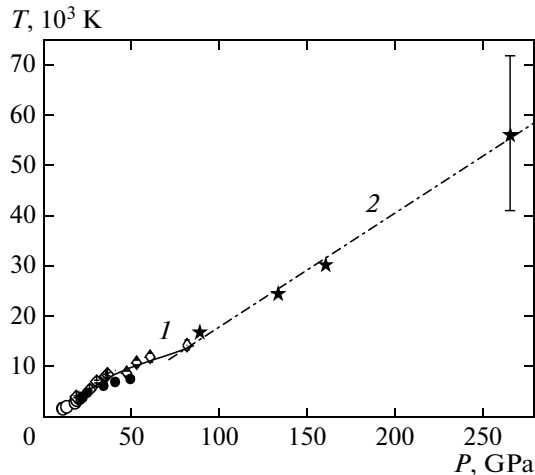


**Fig. 8.** Pressure dependence of the temperature of shock-compressed liquid nitrogen: symbols correspond to experiments (★, ●) our results; (◇) [8]); the curves are the results of approximation ((1) [32]; (2) linear approximation of our results for  $P \approx 90$ –350 GPa).

## 6. DISCUSSION OF EXPERIMENTAL DATA ON THERMODYNAMIC PROPERTIES OF SHOCK-COMPRESSED NITROGEN

### 6.1. Shock Adiat in Kinematic Variables

Our experimental data on shock compression of liquid nitrogen with initial density  $\rho_0 = 0.807$  g/cm³ in the shock wave front velocity range  $12 \text{ km/s} \leq D \leq 20 \text{ km/s}$  were supplemented with the earlier experimental results obtained in [3–8] for a relatively low velocity ( $D \leq 12 \text{ km/s}$ ) and the experimental point of high-intensity shock compression [15] ( $D = 22.9 \text{ km/s}$ , mass velocity  $U = 17.4 \text{ km/s}$ ). The results of all experiments are shown in Fig. 10 in kinematic coordinates. Three regions can clearly be distinguished. In the region of relatively low mass velocities ( $1 \text{ km/s} < U < 4.5 \text{ km/s}$ ), the experimental points can be described with a confidence level of 90% by a linear dependence (line 1 in Fig. 10)

$$D = 1.572 + 1.365 U. \quad (1)$$

In the intermediate region ( $4.17 \text{ km/s} < U < 11.3 \text{ km/s}$ ), the experimental data can be approximated by a slightly nonlinear dependence (curve 2 in Fig. 10)

$$D = -2.008 + 3.375 U - 0.337 U^2 + 0.015 U^3. \quad (2)$$

In the range of high velocities ( $U \geq 11.3 \text{ km/s}$ ), the experimental data can again be approximated by a linear dependence (line 3)

$$D = -1.174 + 1.407 U. \quad (3)$$

The results of this study and of previous experiments now cover the entire interval of shock compressions up to  $D \leq 22 \text{ km/s}$  ( $P \leq 320 \text{ GPa}$ ). It can be seen that the results of all experiments are in good agreement and that the shock adiabat clearly contains three

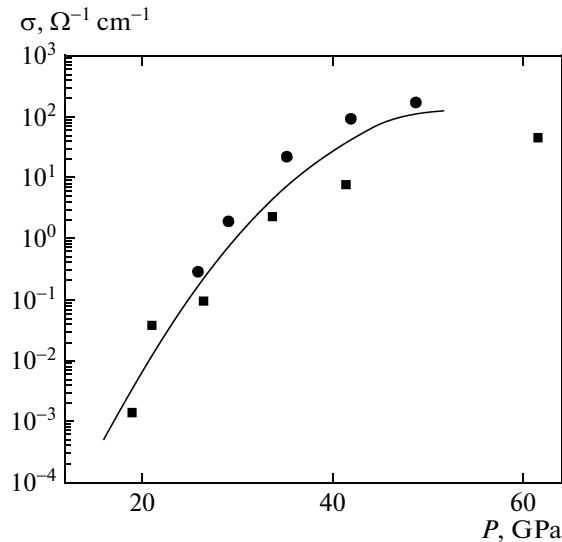


**Fig. 9.** Conductivity of liquid nitrogen as a function of pressure: symbols correspond to experiments ((●) our results; (■) [6, 8]); the curve is the result of approximation.



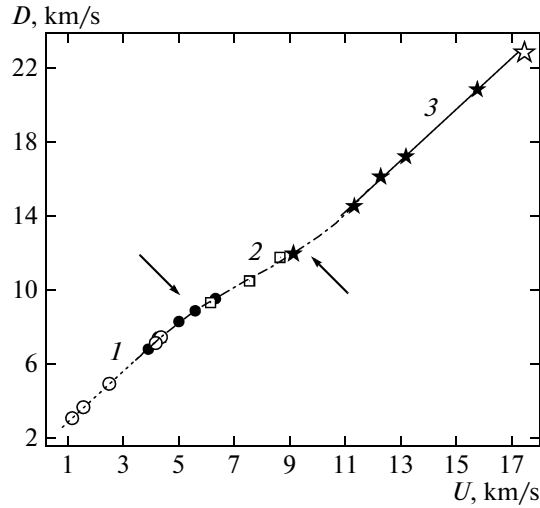


**Fig. 10.** Kinematic characteristics of shock compression of liquid nitrogen,  $\rho_0 = 0.807 \text{ g/cm}^3$  ( $D$  and  $U$  are the velocity of the shock wave front and the mass velocity); bold arrows indicate predicted transitions from the zone of molecular state (1) to the polymer state (2) and then to the state of a nonideal plasma (3); symbols correspond to experiment ((● and ★) our results, plane and spherical waves, respectively; (○) [3], (□) [8], (☆) [15]); curves 1–3 are the results of approximation by dependences (1), (2), and (3), respectively.

segments with different slopes of the  $D(U)$  curve:  $D \leq 9 \text{ km/s}$ ,  $9 \text{ km/s} \leq D \leq 13 \text{ km/s}$ , and  $13 \text{ km/s} \leq D \leq 22 \text{ km/s}$ . Available information allows up to attribute these three segments to the regions with different predominant structural states of nitrogen: purely molecular nitrogen in the first region, predominantly polymer nitrogen in the second region, and completely dissociated and partly or completely ionized nitrogen in the third region (see analysis of the model calculations below). Thus, our experiments make it possible to localize the approximate position of the “depolymerization” zone on the shock adiabat of nitrogen, i.e., the boundaries between its polymer state and dissociated and partly ionized state, viz., pressure-induced ionization boundary:  $D \approx 12 \text{ km/s}$  ( $P \approx 90 \text{ GPa}$  and  $\rho \approx 3.5 \text{ g/cm}^3$ ,  $v \approx 8 \text{ cm}^3/\text{mol}$ ).

## 6.2. Shock Adiabat for Nitrogen in Pressure–Density Variables

The results of all experiments in pressure  $P$  vs. density  $\rho$  coordinates are shown in Fig. 11. As in the case of the  $D(U)$  dependence, it can be seen that the shock adiabat clearly contains three segments with different behaviors of the  $P(\rho)$  dependence: the region of relatively low shock pressures ( $P \leq 50 \text{ GPa}$ ) changes to a region of intermediate pressure values ( $50 \text{ GPa} \leq P \leq 100 \text{ GPa}$ ) with a relatively low slope of the  $P(\rho)$  dependence, which apparently corresponds to the polymer structure of dense fluid nitrogen. Finally, in the range

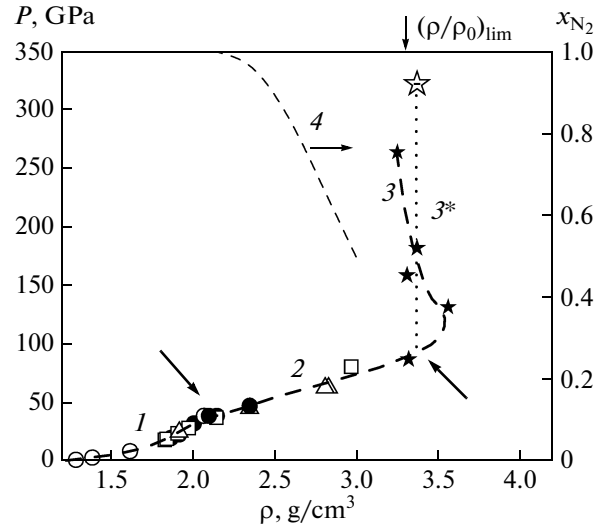


**Fig. 11.** Thermodynamic characteristics of shock compression of liquid nitrogen,  $\rho_0 = 807 \text{ g/cm}^3$  ( $P$  and  $\rho$  are the pressure and density behind the shock wave front); bold arrows indicate predicted transitions from the zone of molecular state (1) to the polymer state (2) and then to the state of a nonideal plasma (3); symbols correspond to experiment; curves 1 and 3 are the results of approximation (notation is the same as in Fig. 10); 3\* is schematic branch of the adiabat for nitrogen in the region of a nonideal plasma with a nearly constant Grüneisen parameter  $\text{Gr} = V(\partial P/\partial E)_V \approx 0.62$ ; 4 is calculation of the fraction of  $\text{N}_2$  molecules  $x_{\text{N}_2} \equiv n_{\text{N}_2}/(n_{\text{N}_2} + n_{\text{N}})$  in the SAHA model (see text).

of high pressures ( $P > 100 \text{ GPa}$ ), the form of the  $P(\rho)$  dependence on the shock adiabat sharply changes and becomes close to the typical limiting compression ratio for an ideal monatomic gas:  $(\rho/\rho_0)_{\text{lim}} \approx 4$ . In the pressure range  $P = 120\text{--}130 \text{ GPa}$ , the highest density  $\rho_{\text{max}} \approx 3.6 \text{ g/cm}^3$  of shock-compressed nitrogen was observed in our experiments.

The important conclusion of this study is that, according to our results and those obtained in [15] ( $P = 323 \text{ GPa}$ ,  $\rho = 3.37 \text{ g/cm}^3$ ,  $\rho/\rho_0 \approx 4.16$ ), the new segment of the shock adiabat on the  $P$ – $V$  plane ( $100 \text{ GPa} \leq P \leq 330 \text{ GPa}$ ) is an almost vertical line with a compression ratio of  $\rho/\rho_0 \approx 4.25$ , which is close to the corresponding value for an ideal gas ( $(\rho/\rho_0)_{\text{lim}} \approx 4.0$ ). It should be emphasized that such a behavior of the shock adiabat (i.e.,  $(\partial \rho/\partial P)_{\text{Hug}} \approx 0$ ) on a considerable segment ( $\rho \approx 3.4 \text{ g/cm}^3$ ,  $P = 100\text{--}330 \text{ GPa}$ ) is equivalent, in accordance with the Rankine–Hugoniot equation [34], to a constant Grüneisen thermodynamic parameter  $\text{Gr} \equiv V(\partial P/\partial E)_V \approx 0.62$  (i.e.,  $E(P, V) \approx C_1 PV + C_2$ , where  $C_1, C_2 = \text{const}$ ), which is close to the ideal-gas value of  $V(\partial P/\partial E)_V = 2/3$ . This feature is illustrated in Fig. 12, which shows our experimental points and the point obtained in [15] in internal energy vs. pressure coordinates, as well as the  $E(P)$  dependence on the isochore  $\rho = 3.4 \text{ g/cm}^3$  calculated using the SAHA model (see below). It is remarkable

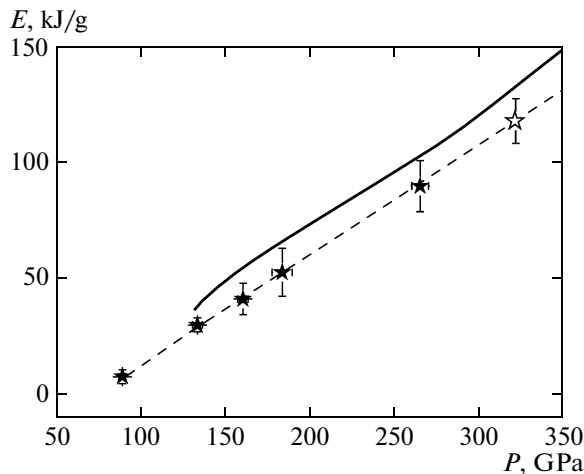


**Fig. 12.** High-temperature (plasma) segment of the shock adiabat for nitrogen (domain of approximately constant Grüneisen parameter  $Gr \approx 0.62$ , dashed line); energy zero is the energy of an ideal atomic gas at  $T = 0$  K; symbols correspond to experiments (( $\star$ ) our results (see Table 2); ( $\star$ ) [15]); solid curve is the internal energy of a nonideal nitrogen plasma calculated in the SAHA model along the isochore  $\rho \approx 3.4$  g/cm<sup>3</sup>.

that, in spite of a slight spread in experimental points on the density scale, all points fit to a high degree of accuracy the linear dependence

$$E(P, V) \approx 1.62PV + \text{const.} \quad (4)$$

This fact is important since it allows us to directly verify the ability of various approximate theoretical models to correctly describe the thermodynamics of shock-compressed nitrogen in the state of a dense strongly nonideal partly ionized plasma with temperature  $T = (20-60) \times 10^3$  K according to our calculations and the value of Coulomb nonideality parameter  $\Gamma_D \equiv e^2/kTr_D \geq 1$  ( $e$  is the electron charge and  $r_D$  is the Debye radius).

### 6.3. Measurement of Temperature on the Shock Adiabat

Figure 8 (see above) shows the results of measurements of temperature in experiments of shock compression as a function of pressure. It can be seen from the figure that our experimental results, as well as the data obtained in [8], are in good agreement with each other and with the results of calculations [32] up to pressures of approximately 90 GPa. The temperatures of shock-compressed liquid nitrogen at higher pressures were obtained for the first time.

## 7. COMPARISON OF EXPERIMENTAL DATA WITH THE RESULTS OF THEORETICAL CALCULATIONS

In Fig. 13, the data on shock compression of liquid nitrogen are compared with the results of calculations performed using numerical codes SAHA and CCM

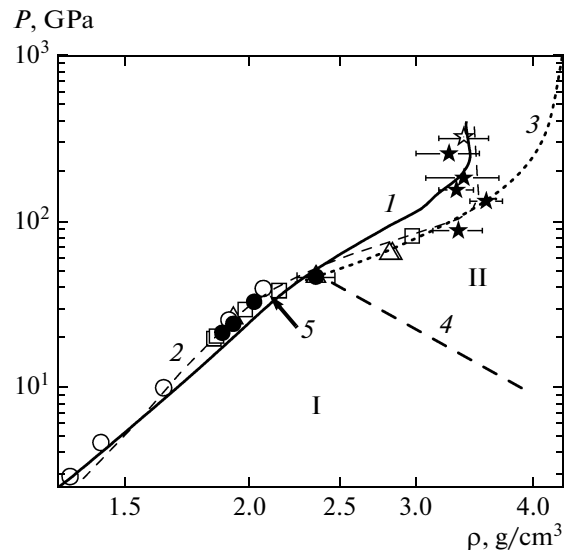


**Fig. 13.** Shock adiabat for a dense nitrogen plasma ( $\rho \approx 0.807$  g/cm<sup>3</sup>); symbols correspond to experiment (notation is the same as in Fig. 10); curves are theoretical calculations (1) using the SAHA model for a nonideal plasma, (2) by interpolating CCM [15, 38], and (3) using the interpolating model from [12] up to the maximal compression point  $(\rho/\rho_0)_{\text{lim}} \approx 5.25$ ; (4) predicted position of the polymerization boundary for molecular nitrogen in the liquid phase [12]; (5) position of this boundary on the shock adiabat according to [21] (see review [19]); I and II are the zones of molecular and polymer state of nitrogen, respectively.

based on two theoretical models: SAHA [35, 36] and CCM [37, 38]. Both approximations are to a certain extent versions of the so-called chemical model of plasma (see, for example, [39]) describing dense fluid nitrogen as a partly ionized thermodynamically equilibrium mixture of atoms, molecules, atomic and molecular ions, and electrons.

### 7.1. Calculations Based on the SAHA Model

In the former case, we used the version of the chemical model which was successfully employed for describing shock compression of molecular hydrogen [25, 40]. In this approach, the initial assumptions and the description are constructed at a microscopic level [36]. A nitrogen plasma is described as a strongly nonideal multicomponent mixture of ions, electrons, atoms, and molecules, as well as  $N^-$  and  $N_2^+$  ions with a strong Coulomb interaction and high-intensity short-range repulsion of heavy particles and with partial degeneracy of electrons. The contribution from the Coulomb nonideality in the calculation of the equilibrium composition and thermodynamic functions, as well as shock compression parameters (Hugoniot adiabat), is described using the modified pseudopotential approximation [41]. In this modification, the effective electron-ion interaction is

described by the Coulomb potential corrected at short distances between charges (Glauber pseudopotential [42, 43]). The effective depth of this potential is equated to the energy of interaction of an electron-ion pair for the average distance between heavy particles (ions, atoms, and molecules). This corresponds to the boundary energy adopted in the given model, which separates free and bound (intratomic) states taken into account in the calculation of statistical sums for nitrogen atoms.

In addition to the contribution from the Coulomb interaction between heavy particles, we took into account the effect of intense repulsion of heavy particles at short distances [36]. The contribution of such a repulsion can be described using the approximate equation of the state in the "soft sphere" model [44], modified in our study to the case of a multicomponent mixture with substantially different intrinsic volumes ("diameters") of particles. This difference leads to an effective shift in chemical and ionization equilibria, which is taken into account in terms of effective "corrections to nonideality" for the equilibrium chemical potentials of particles. In the approach discussed here, the key point is the choice of the relation between the intensities of intermolecular and interatomic repulsions [25, 36, 45] (see [46] for details). The calculations performed in the SAHA approximation demonstrated, in addition to the leading role of the interaction between molecules  $N_2 \rightleftharpoons N$ , the high sensitivity of the position of shock adiabats of the nitrogen plasma and the form of the temperature dependence on these adiabats to the choice of parameters of repulsion between nitrogen atoms ( $N \rightleftharpoons N$ ) and especially between nitrogen atoms and molecules ( $N \rightleftharpoons N_2$ ).

In these calculations (part of the results are given above in Table 1), a priori indeterminate characteristics of repulsion in molecule-molecule, atom-molecule, and atom-atom vapors were chosen as close as possible to the values obtained in accordance with the recommendations of the strictly nonempirical atom-atom approximation [19, 21, 24]. In terms of the soft sphere model, this leads to relatively high values of the ratio of effective diameter  $D_N$  of the nitrogen atom to diameter  $D_{N_2}$  of the nitrogen molecule:  $D_N/D_{N_2} \approx 0.58$ . An important consequence of such a choice is the relatively noticeable change (decrease) in the intrinsic volume of dissociation products of nitrogen molecules. This leads to a noticeable effect of the mechanism stimulating the strongly compressed equilibrium system of molecules and atoms and to pressure-induced dissociation due to the above-mentioned gain in intrinsic volume.

The model described here was implemented in the universal SAHA-IV code [39, 47], which is a modification of the SAHA family of codes [35] constructed for describing a multicomponent strongly nonideal plasma in a wide range of parameters. In accordance with the results of calculations based on this code, in

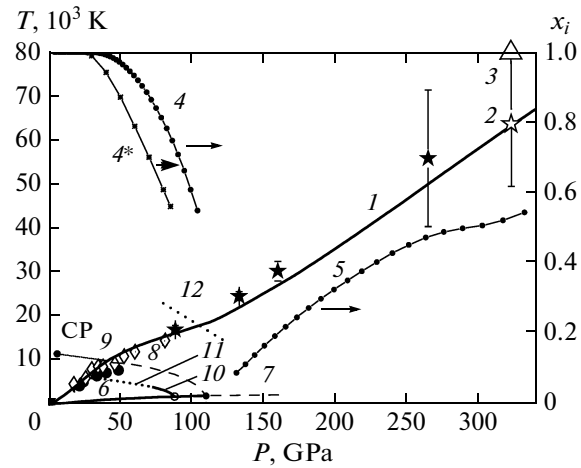


**Fig. 14.** Temperature of a shock-compressed nitrogen plasma as a function of pressure; comparison of theory and experiments: symbols correspond to experiments (( $\star$ ,  $\bullet$ ) our results; ( $\star$ ) [8]); the curves are (1) the results of calculation using the SAHA model for a nonideal plasma; see text; (2) predicted temperature of the state attained in experiment [15] as an extrapolation of our calculations based on the SAHA model to the pressure level  $P = 323$  GPa attained in [15]; (3) estimate of temperature of the state attained in [15] in accordance with calculation based on the CCM; (4) fraction of molecules  $x_{N_2} \equiv n_{N_2}/(n_{N_2} + n_N)$  and (5) degree of ionization  $x_{N^+} \equiv n_{N^+}/(n_{N^+} + n_N)$  of nitrogen atoms according to our calculations based on the SAHA model disregarding the polymer phase; (4\*) fraction of molecules [32]; (6) melting boundary of the molecular crystal [12, 23]; (7) extrapolation of the melting boundary; (8) predicted boundary of the transition from the molecular phase of liquid nitrogen (bottom) to the polymer phase (top) [12]; CP is the critical point of the first-order phase transition from the molecular phase of liquid nitrogen to the polymer phase [19, 21]; (9) extrapolation of boundary 8 to the critical point [19]; (10) boundary of the first-order phase transition from the molecular to polymer phase in liquid nitrogen according to calculations in quantum molecular dynamics [23]; (11) the same as a continuous transition [23]; (12) predicted boundary of transition from the polymer state of liquid nitrogen (bottom) to the state of a nonideal plasma (top) according to our experiments.

our experiments, as well as in the experiment [15] with the highest pressure, the state of a dense strongly nonideal ( $\Gamma_D \gg 1$ ) partly ionized ( $n_e/n_a \approx 1$ ) and partly degenerate ( $n_e \lambda_e^3 \approx 3$ ) plasma with parameters given above in Table 3 is formed behind the shock wave front (here,  $n_e$  and  $n_a$  are the concentrations of electrons and atoms per unit volume and  $\lambda_e$  is the de Broglie wavelength).

## 7.2. Calculations Based on the "Compressible Covolume Model" (CCM)

In the second version, which is semiempirical to a larger extent, calculations of the equation of state of a

dense nitrogen fluid [15] were performed using the code based on a relatively simple compressible covolume model (CCM) [37, 38]. As in the SAHA model, calculations were carried out for a mixture of five species of particles ( $N_2$ ,  $N$ ,  $N_2^+$ ,  $N^+$ , and electrons), the equilibrium compositions of which were determined from the condition of the free energy minimum of the system. The statistical sums of excitation of molecules and molecular ions were described in the rigid rotator–harmonic oscillator approximation. The basic element of this approach is the use of an individual intrinsic volume (covolume)  $V_i$  for each species of particles, which was chosen semiempirically (see [48] for details). Covolumes  $V_i$  we assumed to be additive and functions of pressure. The electron covolume was set to zero. The covolumes for atomic ( $N^+$ ) and molecular ( $N_2^+$ ) ions we assumed to be equal to the covolumes of atoms  $N$  and molecules  $N_2$ ; consequently, in this approximation, only covolumes of  $N_2$  molecules and  $N$  atoms and their dependence on pressure must actually be specified. Both of these covolumes were represented by simple function of pressure and their free parameters were chosen in accordance with considerations of the best possible description of the results of shock experiments [3, 5, 6, 15].

## 8. DISCUSSION

### 8.1. Shock Adiat for Nitrogen in Pressure–Density Variables

Figure 13 shows the results of calculation of the shock adiabat for liquid nitrogen in  $P$ – $\rho$  coordinates using the above two versions of the equation of state. It can be seen that the dependences calculated using the SAHA and CCM codes are generally in satisfactory agreement with experiment and reflect its typical features. The CCM code provides a better description of the entire body of experimental data in view of the semiempirical nature of the CCM [38] and its higher “flexibility” in the interpolation description of experimental data due to appropriate selection of the required empirical dependence of the atomic and molecular covolumes on pressure [15]. Analysis shows that the shock adiabats given by the above theoretical models in the limit of high pressures and temperatures tend to the asymptotic limit corresponding to ideal gas compression ratio  $\rho/\rho_0 \rightarrow 4$ ; however, the forms of this tendency in the CCM and SAHA models differ significantly. This necessitates obtaining new experimental data in the pressure range 2–10 Mbar as well as the use of rigorous ab initio approaches to calculation of thermodynamic functions for dense nitrogen plasmas for comparison with experiment. This approach (methods of density functional for electrons and molecular dynamics for ions) was used recently [23] and led to very important results in the low-temperature region.

### 8.2. Shock Adiat for Nitrogen in Pressure–Temperature Variables

Calculations based on the SAHA model correctly reproduce the results of measurements of temperature [5, 14] along the main shock adiabat (Fig. 14). This stimulates the calculation of the shock adiabat based on rigorous ab initio approaches using the methods of density functional and continuous integrals. In addition to calculations based on the SAHA code, Fig. 14 shows the estimates of the temperature attained in experiment [15] in accordance with calculations based on the CCM model (see Section 7.2), as well as the extrapolation of the  $P(T)$  dependence on the shock adiabat, calculated in the SAHA model, to the value of pressure measured in [15].

Figure 14 contains information on the composition (degrees of dissociation and ionization) and the extent of nonideality of the plasma along the shock adiabat according to our calculations based on the SAHA code. The illustrations of the available estimates and calculations of the boundary separating the domains of the hypothetical polymer phase of liquid and solid nitrogen from the domains of molecular (liquid and solid) nitrogen are very important. The critical point of this transition predicted in pioneering works [19, 21, 22] is in good agreement with the estimates of this boundary from [12]. These preliminary results are refined in recent calculations using the molecular dynamics method [23], which predict that this boundary corresponds to the first-order phase transition at  $T \leq 2000$  K and to a blurred phase transition at  $2000 \text{ K} \leq T \leq 4000$  K. The main result of the present study based on the above-mentioned clearly manifested kink on the shock adiabat at  $P \approx 100$  GPa is the assumption that, for these parameters (line 12 in Fig. 14), depolymerization takes place and is accompanied by an increase in the degree of ionization and in the extent of nonideality of the nitrogen plasma as a new form of pressure-induced ionization observed for hydrogen (deuterium) and inert gases [25].

## 9. CONCLUSIONS AND PROSPECTS

Analysis of the properties of shock-compressed nitrogen led to important characteristics of a nonideal nitrogen plasma in the pressure range  $P = 100$ – $265$  GPa. The advantage of the experiments was simultaneous measurement of the compression ratio, pressure, and temperature of the nitrogen plasma. The values of temperature were obtained under the assumption that the radiation spectrum of the shock wave front is continuous in the wavelength range under investigation.

In the pressure range of 100–130 GPa, the strongest compression of nitrogen was observed. According to our measurements and the earlier experiment [15], the  $P(\rho)$  dependence on the shock adiabat at pressures above 160 GPa acquires a remarkable nearly isochoric

form with a compression ratio of  $\rho/\rho_0 \approx 4.2$ , which is close to the ideal-gas value ( $\rho/\rho_0 \approx 4$ ) in a wide pressure range  $100 \text{ GPa} \leq P \leq 330 \text{ GPa}$ . Such a behavior of the shock adiabat was observed for the first time. It indicates the existence of a wide range of nitrogen plasma parameters with a nearly constant Grüneisen parameter  $Gr \equiv V(\partial P/\partial E)_V \approx 0.62$ . This property can be useful for a direct verification of applicability of various theoretical models of the equation of state for nonideal plasmas of molecular gases. The experimental and theoretical results obtained here together with the results of previous calculations and experiments lead to the conclusion that parameters  $P \approx 100 \text{ GPa}$ ,  $T \approx 16000 \text{ K}$ , and  $\rho \approx 3.3 \text{ g/cm}^3$  correspond to the termination of depolymerization in nitrogen and its transition to the state of a dense nonideal plasma.

### ACKNOWLEDGMENTS

The authors are grateful to E.S. Yakub and L.N. Yakub for providing the results of their works on the thermodynamics of polymerization in shock-compressed nitrogen and for fruitful discussions.

This study was supported by the program "Thermal Physics and Mechanics of Extreme Energy Effects and Physics of Strongly Compressed Matter" of the Presidium of the Russian Academy of Sciences.

### REFERENCES

1. V. E. Fortov, *Usp. Fiz. Nauk* **179** (6), 653 (2009) [Phys.—Usp. **52** (6), 657 (2009)].
2. A. A. Radtsig and B. M. Smirnov, *Handbook on Atomic and Molecular Physics* (Atomizdat, Moscow, 1980) [in Russian].
3. V. N. Zubarev and G. S. Telegin, *Dokl. Akad. Nauk SSSR* **142**, 309 (1962) [Sov. Phys. Dokl. **7**, 34 (1962)].
4. I. M. Voskoboinikov, M. F. Gogulya, and A. Yu. Dolgoborodov, *Dokl. Akad. Nauk SSSR* **246**, 579 (1979) [Sov. Phys. Dokl. **24**, 375 (1979)].
5. W. Nellis and A. Mitchell, *J. Chem. Phys.* **73**, 6137 (1980).
6. H. B. Radousky, W. J. Nellis, M. Ross, D. C. Hamilton, and A. C. Mitchell, *Phys. Rev. Lett.* **57**, 2419 (1986).
7. H. B. Radousky and M. Ross, *High Pressure Res.* **1**, 39 (1988).
8. W. J. Nellis, H. B. Radousky, D. C. Hamilton, A. C. Mitchell, N. C. Holmes, K. B. Christianson, and M. van Thiel, *J. Chem. Phys.* **94**, 2244 (1991).
9. F. V. Grigor'ev, S. B. Kormer, O. L. Mikhailova, M. A. Mochalov, and V. D. Urlin, *Zh. Éksp. Teor. Fiz.* **88** (4), 1271 (1985) [Sov. Phys. JETP **61** (4), 751 (1985)].
10. *The Properties of Condensed Materials at High Pressures and Temperatures*, Ed. by R. F. Trunin (Russian Federal Nuclear Centre—All-Russian Scientific-Research Institute of Experimental Physics, Sarov, Russia 1992) [in Russian].
11. L. V. Al'tshuler, R. F. Trunin, K. K. Krupnikov, and N. V. Panov, *Usp. Fiz. Nauk* **166** (5), 575 (1996) [Phys.—Usp. **39** (5), 539 (1996)].
12. M. Ross and F. Rogers, *Phys. Rev. B: Condens. Matter* **74**, 024103 (2006).
13. V. K. Gryaznov, M. V. Zhernokletov, I. L. Iosilevskii, et al., in *Proceedings of the Seventh Kharitonov Topical Scientific Readings*, Ed. by A. L. Mikhailov (Russian Federal Nuclear Centre—All-Russian Scientific-Research Institute of Experimental Physics, Sarov, Russia 2005), p. 326.
14. N. F. Gavrilov, G. G. Ivanova, V. I. Selin, et al., *Vopr. At. Nauki Tekh., Ser.: Metod. Programmy Chislennogo Resheniya Zadach Mat. Fiz.*, No. 3, 11 (1982).
15. R. F. Trunin, G. V. Boriskov, A. I. Bykov, A. B. Medvedev, G. V. Simakov, and A. N. Shuikin, *Pis'ma Zh. Éksp. Teor. Fiz.* **88** (3), 220 (2008) [JETP Lett. **88** (3), 189 (2008)].
16. E. N. Avrorin, B. N. Vodolaga, V. A. Simonenko, and V. E. Fortov, *Usp. Fiz. Nauk* **163** (5), 1 (1993) [Phys.—Usp. **36** (5), 337 (1993)].
17. V. E. Fortov, A. G. Khrapak, and I. T. Yakubov, *Physics of Nonideal Plasma*, (Fizmatlit, Moscow, 2004) [in Russian].
18. M. I. Eremets, A. G. Gavriluk, N. R. Serebryanaya, I. A. Trojan, D. A. Dzivenko, R. Boehler, H. K. Mao, and R. J. Hemley, *J. Chem. Phys.* **121**, 11 296 (2004).
19. E. S. Yakub, *Fiz. Nizk. Temp. (Kharkov)* **19** (5), 531 (1993) [Low Temp. Phys. **19** (5), 377 (1993)].
20. M. Ross, *J. Chem. Phys.* **86**, 7110 (1987); *High Pressure Res.* **10**, 649 (1992).
21. E. S. Yakub, *Zh. Fiz. Khim.* **67**, 305 (1993).
22. L. N. Yakub, *Fiz. Nizk. Temp. (Kharkov)* **19**, 531 (1993).
23. B. Boates and S. A. Bonev, *Phys. Rev. Lett.* **102**, 015701 (2009).
24. E. S. Yakub, *Teplofiz. Vys. Temp.* **28**, 664 (1990).
25. V. E. Fortov, V. Ya. Ternovoi, M. V. Zhernokletov, M. A. Mochalov, A. L. Mikhailov, A. S. Filimonov, A. A. Pyalling, V. B. Mintsev, V. K. Gryaznov, and I. L. Iosilevskii, *Zh. Éksp. Teor. Fiz.* **124** (2), 288 (2003) [JETP **97** (2), 259 (2003)].
26. G. G. Ivanova and T. A. Mikiichuk, *Vopr. At. Nauki Tekh., Ser.: Mat. Model. Fiz. Protssessov*, No. 1, 43 (1992).
27. D. G. Gordeev, L. F. Gudarenko, M. V. Zhernokletov, V. G. Kudel'kin, and M. A. Mochalov, *Fiz. Goreniya Vzryva* **44** (2), 61 (2008) [Combust., Explos. Shock Waves **44** (2), 177 (2008)].
28. A. A. Evstigneev, M. V. Zhernokletov, and V. N. Zubarev, *Fiz. Goreniya Vzryva* **12** (5), 758 (1976) [Combust., Explos. Shock Waves **12** (5), 678 (1976)].
29. B. L. Glushak, L. F. Gudarenko, and Yu. M. Styazhkin, *Vopr. At. Nauki Tekh., Ser.: Mat. Model. Fiz. Protssessov*, No. 2, 57 (1991).
30. M. V. Zhernokletov, T. S. Lebedeva, A. B. Medvedev, M. A. Mochalov, A. N. Shuykin, and V. E. Fortov, in *Shock Compression of Condensed Matter*, Ed. by M. D. Furnish, N. N. Thadhani, and Y. Horie, (American Institute of Physics, New York, 2001), p. 763.

31. M. Boslaff and T. Arens, *Prib. Nauchn. Issled.*, No 12, 52 (1989).
32. D. F. Calef and F. H. Ree, *Phys. Rev. B: Condens. Matter* **36**, 4935 (1987).
33. L. A. Gatilov and L. V. Kuleshova, *Prikl. Mekh. Tekh. Fiz.*, No. 1, 136 (1981).
34. Ya. B. Zel'dovich and Yu. P. Raizer, *Physics of Shock Waves and High-Temperature Hydrodynamic Phenomena* (Academic, New York, 1966; Fizmatlit, Moscow, 2008).
35. V. K. Gryaznov, I. L. Iosilevskii, Yu. G. Krasnikov, N. I. Kuznetsova, V. I. Kucherenko, G. B. Lappo, B. N. Lomakin, G. A. Pavlov, E. E. Son, and V. E. Fortov, *Thermophysical Properties of Working Media in a Gas-Phase Nuclear Reactor*, Ed. by V. M. Ievlev (Atomizdat, Moscow, 1980) [in Russian].
36. V. K. Gryaznov, I. L. Iosilevskii, and V. E. Fortov, in *High Pressure Shock Compression*, Vol. VII: *Shock Waves and Extreme States of Matter*, Ed. by V. E. Fortov, L. V. Al'tshuler, R. F. Trunin, and A. I. Funtikov (Nauka, Moscow, 2000; Springer, New York, 2004), p. 299.
37. A. B. Medvedev, *Vopr. At. Nauki Tekh., Ser.: Teor. Prikl. Fiz.*, No. 1, 23 (1990).
38. A. B. Medvedev, in *High Pressure Shock Compression*, Vol. VII: *Shock Waves and Extreme States of Matter*, Ed. by V. E. Fortov, L. V. Al'tshuler, R. F. Trunin, and A. I. Funtikov (Nauka, Moscow, 2000; Springer, New York, 2004), p. 315.
39. V. K. Gryaznov, I. L. Iosilevskii, and V. E. Fortov, in *Encyclopedia of Low-Temperature Plasma*, Ed. V. E. Fortov (Fizmatlit, Moscow, 2004), Vol. Suppl. III-1, p. 111 [in Russian].
40. S. K. Grishechkin, S. K. Gruzdev, V. K. Gryaznov, M. V. Zhernokletov, R. I. Il'kaev, I. L. Iosilevskii, G. N. Kashintseva, S. I. Kirshanov, S. F. Manachkin, V. B. Mintsev, A. L. Mikhailov, A. B. Mezhevov, M. A. Mochalov, V. E. Fortov, V. V. Khrustalev, A. N. Shukin, and A. A. Yukhimchuk, *Pis'ma Zh. Éksp. Teor. Fiz.* **80** (6), 452 (2004) [*JETP Lett.* **80** (6), 398 (2004)].
41. I. L. Iosilevskii, in *Encyclopedia of Low-Temperature Plasma*, Ed. V. E. Fortov (Fizmatlit, Moscow, 2004), Vol. Suppl. III-1, p. 349 [in Russian].
42. A. E. Glaubergerman, *Dokl. Akad. Nauk SSSR* **78**, 883 (1951).
43. I. L. Iosilevskii, *Teplofiz. Vys. Temp.* **18**, 447 (1980) [*High Temp.* **18**, 355 (1980)].
44. D. Young, Preprint No. UCRL-52352 (Lawrence Livermore National Laboratory (LLNL), University of California, California, United States, 1977); G. R. Gather, J. W. Shaner, R. S. Hixon, and D. A. Young, *Rep. Prog. Phys.* **49**, 341 (1986).
45. I. L. Iosilevskii, V. K. Gryaznov, and V. E. Fortov, in *Physics of the Extreme States of Matter*, Ed. by V. E. Fortov (Institute of Problems of Chemical Physics, Chernogolovka, Russia, 2001), p. 114 [in Russian].
46. W. Ebeling, A. Förster, V. Fortov, V. Gryaznov, and A. Polishchuk, *Thermophysical Properties of Hot Dense Plasmas* (Teubner, Stuttgart, 1991; *Regulyarnaya i Khaoticheskaya Dinamika*, Moscow, 2007).
47. V. K. Gryaznov, in *Encyclopedia of Low-Temperature Plasma*, Ed. V. E. Fortov (Nauka, Moscow, 2004), Vol. 1, p. 299 [in Russian].
48. V. P. Kopyshev, A. B. Medvedev, and V. V. Khrustalev, in *Encyclopedia of Low-Temperature Plasma*, Ed. V. E. Fortov (Fizmatlit, Moscow, 2004), Vol. Suppl. III-1, p. 59 [in Russian].
49. R. Chau, A. Mitchell, R. Minich, and W. Nellis, *Phys. Rev. Lett.* **90**, 245501 (2003).

*Translated by N. Wadhwa*